

# Integrated unmanned aerial vehicle platform with sensing and sampling systems for the measurement of air pollutant concentrations

Chen-Wei Liang<sup>1,2</sup>, Chang-Hung Shen<sup>1</sup>

<sup>1</sup> Master Program in UAV Application and Smart Agriculture, National Ilan University, Yilan, Taiwan.

<sup>2</sup> Department of Biomechatronic Engineering, National Ilan University, Yilan, Taiwan.

Correspondence: Chen-Wei Liang (cwliang@niu.edu.tw)

## Abstract

In this study, an unmanned aerial vehicle (UAV) platform with sensing and sampling systems was developed for three-dimensional (3D) measurements of air pollutant concentrations. The sensing system of this platform contains multiple microsensors and Internet of Things devices for determining the 3D distributions of four critical air pollutants and two meteorological parameters in real time. Moreover, the sampling system comprises remote-controllable gas sampling kits, each of which contains a Tedlar bag of 1 L for the 3D measurement of volatile organic compound concentrations according to the TO-15 method of the US Environmental Protection Agency. The performance of the developed UAV platform was verified in experiments where it was used to detect air pollutant emissions from a large industrial zone in Taiwan that included a traditional industrial park, a precision machinery park, and a municipal waste incineration plant. Three locations were selected as field measurement sites according to the prevailing local wind direction. The vertical distributions of four critical air pollutants, ambient temperature, and relative humidity were determined from data gathered at the aforementioned sites in March and May 2023. A total of 56 and 72 chemical species were qualitatively and quantitatively analyzed in these two periods, respectively. The experimental results verified the feasibility of using the proposed UAV platform for accurately evaluating the air pollutant concentration distribution and transport in an industrial zone. The sampling system can be used as a sampling part of the Method To-15, thus extending the method to measure the 3D distribution of VOCs in an area. The UAV platform can serve as a useful tool in the management and decision-making process of air pollution in industrial areas.

**Keywords:** Remote sensing, Low-altitude sampling, EPA method TO-15, Atmospheric monitoring, Vertical profiles, Low-cost microsensors, Particulate matter, Volatile organic compounds

## 1 Introduction

Unmanned aerial vehicle (UAV) remote sensing technology has been widely used in a variety of fields, such as defense, agricultural monitoring, surveying and mapping management, and disaster emergency response management (Yang et al., 2022), especially in the defence field (Zhu et al., 2021). This technology is also used in environmental monitoring to determine the distributions of pollutants, especially air pollutants (Liu et al., 2020; Zheng et al., 2021; Shen et al., 2022; Sun et al., 2023). Fumian et al. (2021) used an UAV platform with metal oxide and photo-ionization detectors to confirm the presence of specific classes of chemicals in a contaminated area. UAV systems for air quality monitoring are inexpensive and allow for high-spatiotemporal-resolution data on air pollutant

38 concentrations to be gathered over a large area (Gu et al., 2018). Cozma et al. (2022) proposed an  
39 autonomous multirotor aerial platform for the real-time, high-resolution monitoring of air quality in  
40 large cities by the obtained fine-grained heat-maps. Duangsuwan et al. (2022) used a UAV system  
41 capable of real-time air pollution monitoring and a machine learning method to obtain a three-  
42 dimensional (3D) air quality index (AQI) map of an area. Samad et al. (2022) developed a low-cost,  
43 practical, and reliable UAV system for the high-resolution 3D profiling of air pollutants at a roadside  
44 area. Galle et al. (2021) used a multirotor UAV to obtain in-situ measurements of sulfur dioxide (SO<sub>2</sub>),  
45 hydrogen sulfide (H<sub>2</sub>S), and carbon dioxide (CO<sub>2</sub>) concentrations in volcanic gas plumes. De Fazio  
46 et al. (2022) developed a remote-controlled UAV with a wide set of sensors to measure the  
47 concentrations of air pollutants emitted by waste fires. Samad et al. (2022) developed a UAV system  
48 for the 3D profiling of particulate matter (PM), ultrafine particle, and black carbon concentrations.  
49 Suroto et al. (2018) designed a waypoint UAV for automatically determining the ambient carbon  
50 monoxide (CO) and PM concentrations. Arroyo et al. (2022) developed an electrochemical gas  
51 sensing module for a UAV to measure ambient CO, ozone (O<sub>3</sub>), nitrogen monoxide (NO), and  
52 nitrogen dioxide (NO<sub>2</sub>) concentrations. Yungaicela-Naula et al. (2017) used a UAV system and  
53 metaheuristic algorithms to measure air pollutant concentrations and track pollution sources in real  
54 time. Huang et al. (2022) integrated a UAV platform with an X-ray fluorescence analyzer to develop  
55 a high-efficiency system for the rapid detection of heavy metal pollution in soil.

56 UAV remote sensing technology has also been widely used in industrial safety management and  
57 agricultural production. Qiu et al. (2017) used a UAV-based monitoring platform and an artificial  
58 neural network model to conduct atmospheric dispersion simulation for identifying contaminant  
59 sources in a chemical industry park. Xie et al. (2013) proposed a design framework for an emergency  
60 atmospheric monitoring system based on a UAV platform. Their platform has high efficiency, high  
61 flexibility, and a wide monitoring range. Alvarado et al. (2015) developed a low-cost airborne sensing  
62 system based on a UAV platform for monitoring dust particles after blasting at open-pit mine sites.  
63 Rotorcraft UAVs are often used to spray pesticides, and the crop movement caused by the rotor of a  
64 UAV is a crucial indicator of the effectiveness of the spraying (2023). Boursianis et al. (2022)  
65 analyzed the roles of UAV and Internet of Things (IoT) technologies in irrigation, fertilizer application,  
66 pesticide application, weed management, plant growth monitoring, crop disease management, and  
67 field-level phenotyping. Their results indicated that UAV and IoT technologies are two of the most  
68 important technologies for transforming traditional farming practices into precision agriculture  
69 practices. Singh and Sharma (2022) proposed a platform for managing the agricultural crop  
70 information collected by a UAV, which has a high potential for use in agricultural applications such  
71 as crop health monitoring, fertilizer spraying, and pesticide spraying. In addition, UAV with low-cost  
72 Lidar sensor networks can provide continuous area surveillance of large spaces (Fumian et al., 2020).  
73 The UAV with sampling system can collect important samples for subsequent laboratory analysis and  
74 confirm results previously obtained from field measurements (Leitner et al., 2023). Opportunities to  
75 collect samples of environmental contaminants expand the possibility of confirming field  
76 measurements through laboratory analysis (Pounds et al., 2011).

77 Most UAV environmental monitoring systems used in previous studies have contained various  
78 microsensors for measuring air pollutant concentrations. Few studies have proposed designs of UAV-  
79 based atmospheric sampling systems for the qualitative and quantitative analysis of low-altitude gas  
80 samples. The components of atmospheric gas samples, especially volatile organic compounds  
81 (VOCs), can be accurately identified and quantified through a combination of atmospheric sampling  
82 and laboratory analysis. In the present study, a UAV platform with sensing and sampling systems was  
83 developed for the measurement of low-altitude air pollutant concentrations. The developed UAV  
84 platform contains an atmospheric sensing system with various low-cost microsensors for the in-situ  
85 measurements of meteorological parameters and air pollutant concentrations to obtain their vertical  
86 profiles. Moreover, this platform contains a gas sampling system with multiple remote-controllable  
87 gas sampling sets. The gas samples collected by the gas sampling system were analyzed in a  
88 laboratory through gas chromatography–mass spectrometry (GC–MS) by using thermal adsorption  
89 equipment in accordance with the TO-15 method of the US Environmental Protection Agency (EPA).  
90 Finally, the developed UAV platform was verified in field experiments where it collected  
91 measurements in a large industrial zone, which included two industrial parks and a municipal waste  
92 incineration plant; these measurements were used to determine pollution levels and contamination  
93 sources.

## 94 **2 Materials and methodology**

### 95 2.1 Developed UAV platform

96 Figure 1 shows the prototype of the developed UAV platform, which comprises three parts: a  
97 UAV, a sensing system, and a sampling system. The hardware of the platform was constructed using  
98 off-the-shelf consumer parts, and the open-source software Ardupilot was used for flight control and  
99 data fusion. An all-in-one drone remote control solution for long-range, high-definition video  
100 transmission, namely Skydroid H16, was used as the UAV's remote controller. The Pixhawk 6C Flight  
101 Controller was used as the autopilot, and the NEO V2 GPS module was used as the unmanned system  
102 positioning and navigation module because of its high sensitivity and strong resistance to interference.  
103 This module allows for an exact 3D spatial location of the sampling site to better describe the air  
104 quality of large spaces.

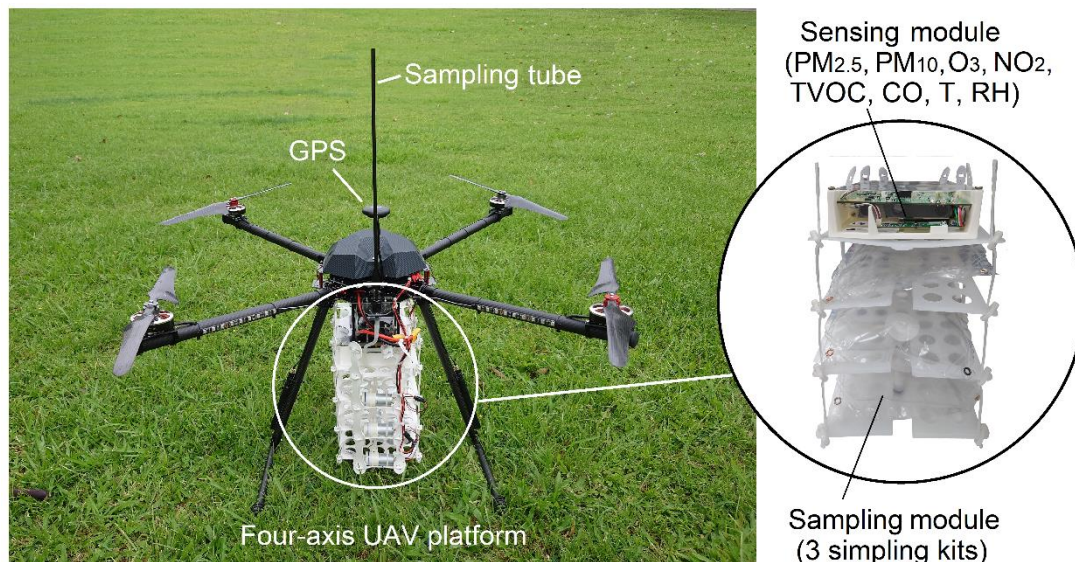


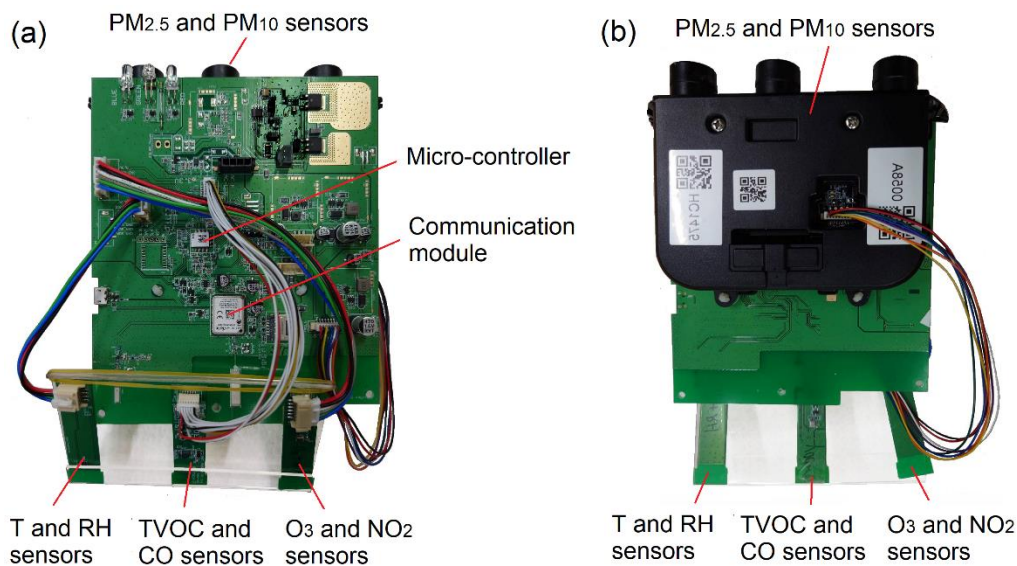
**Figure1.** Prototype of the UAV-based air sensing and air sampling systems.

105  
106

## 107 2.2 Sensing system

108 The use of low-cost microsensors in a UAV platform offers numerous advantages for the  
 109 measurement, especially real-time measurement, of the spatiotemporal distribution of air pollutant  
 110 concentrations (Gu and Jia, 2019; Pochwała et al., 2020). The present study used a low-cost air quality  
 111 monitoring kit (Air Quality Detector II, VISION) as the sensing system in the developed UAV  
 112 platform. This monitoring kit is one of the air quality monitor sensors recommended by the Taiwanese  
 113 Environmental Protection Administration. The parameters monitored with the aforementioned kit  
 114 include PM<sub>2.5</sub> concentration, PM<sub>10</sub> concentration, total VOC (TVOC) concentration, O<sub>3</sub> concentration,  
 115 CO concentration, ambient temperature (T) and relative humidity (RH). The sensing system of the  
 116 developed UAV platform is connected to an IoT system and a cloud server through a communication  
 117 module to track air pollutant concentrations and weather data in real time. The data obtained by the  
 118 microsensors of the sensing system are processed by a microprocessor, and the processed data are  
 119 transferred to a cloud server for storage through Wi-Fi. The data stored on the cloud server can be  
 120 presented in a graphical form in real time. The specifications of the sensing system are listed in Table  
 121 1.





122  
123 **Figure 2.** Circuit board with particulate matter and gas sensors used in the UAV platform. (a) front  
124 and (b) back of the circuit board.

125 **Table 1.** Specifications of sensing module

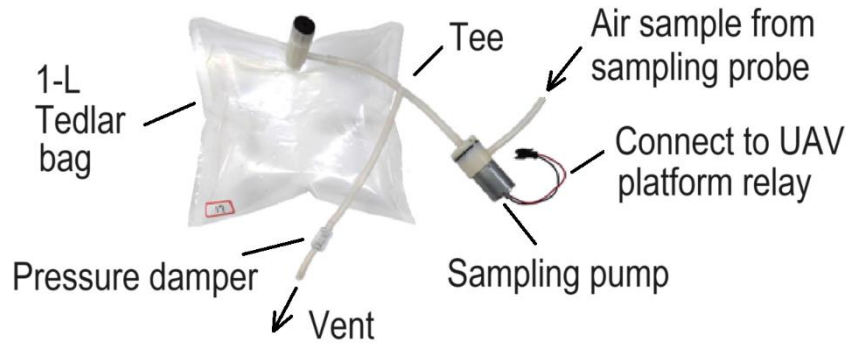
Sensors/devices	Measurement technique/principle	Label/model	Measurement range
T, °C	Bead thermistor	AMS/ENS210	-40 ~ +125
RH, %	Capacitive	AMS/ENS210	0 ~ 100
PM <sub>2.5</sub> /PM <sub>10</sub> , µg/m <sup>3</sup>	Light scattering	VISION/AQ1001	1 ~ 1000
TVOC, ppb	Micro-hot plate technology	AMS/CCS811	0 ~ 29,206
O <sub>3</sub> , ppb	Metal oxide chemiresistor	Renesas/ZMOD4510	20 ~ 500
NO <sub>2</sub> , ppb	Metal oxide chemiresistor	Renesas/ZMOD4510	20 ~ 500
CO, ppm	Metal oxide chemiresistor	SGX/MiCS-5524	0.3 ~ 200
Communication module	–	Telit/ME310G1-WW	–
Micro-controller	–	Nuvoton/M481LIDAE	–

126 Prior to each field measurement run, the PM<sub>2.5</sub>, PM<sub>10</sub>, O<sub>3</sub>, NO<sub>2</sub>, TVOC, CO, T, and RH sensors  
127 had to be calibrated using monitoring data from the Wenshan Air Quality Monitoring Station of the  
128 Taichung City Environmental Protection Bureau (this station is located in the study area; Fig. 4).

### 129 2.3 Sampling system

130 The sampling module contains three gas sampling kits that each comprise three mini air pumps  
131 (TCS Electrical Co. JQC24381), a 1-L Tedlar bag (Keika Ventures), and a plastic one-way check  
132 valve with a compression spring (AliExpress, hose size: 4 mm). This one-way valve was installed in  
133 reverse to act as a pressure damper for the Tedlar bag after sampling by compression spring. Figure  
134 3 shows the scheme of the sampling kit. The three air pumps of the sampling kits are connected in  
135 parallel to a length of 60-cm vertical sampling tube at the top of the UAV. The sampling kits are  
136 powered by the batteries of the UAV platform and are individually controlled by the UAV's remote  
137 controller. Therefore, the sampling system can perform multipoint sampling at different altitudes or  
138 locations in a single flight mission. Multipoint sampling in a single flight can overcome the problem

139 caused by rapidly changing wind fields and makes it easier to obtain representative samples.



140

141 **Figure 3.** Scheme of the sampling kit.

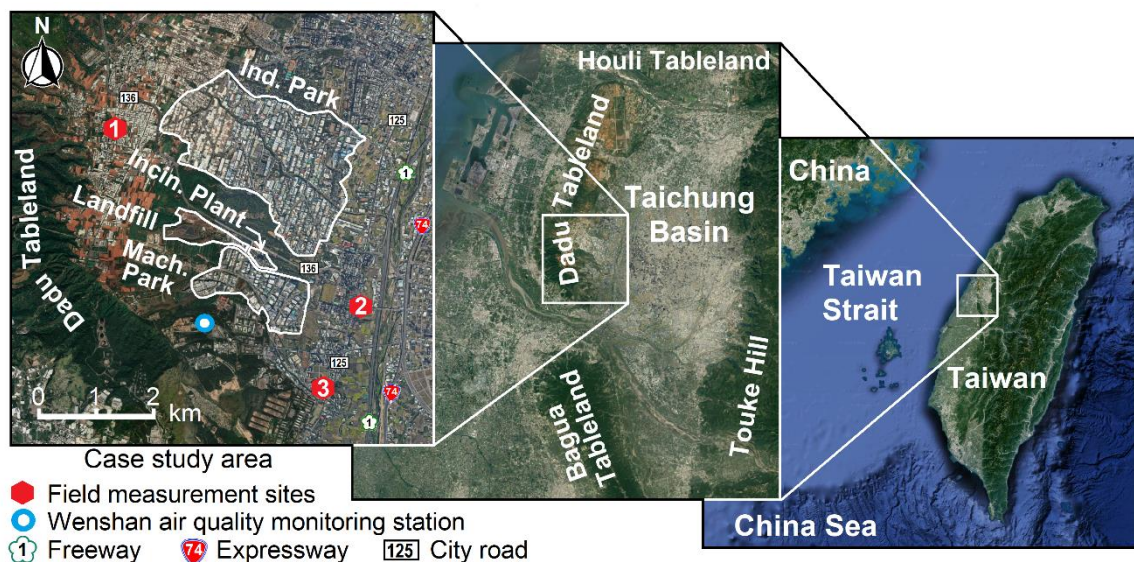
#### 142 2.4 Analysis of high-altitude VOC concentrations

143 The collected gas samples were analyzed in a laboratory in accordance with the TO-15 method  
144 of the US EPA. This method is based on criteria for the sampling and analysis of VOC in air and is  
145 primarily employed for the monitoring of airborne pollutants in urban and industrial environments.  
146 In the TO-15 method, air samples are collected in a special canister. Stainless-steel canisters are too  
147 heavy and bulky and thus are unsuitable for use in the developed UAV platform. Therefore, a 1-L  
148 Tedlar bag is used instead of a stainless-steel canister in the developed UAV platform. Ambient VOCs  
149 were collected in a 1-L Tedlar bag and analyzed by using GC-MS (Shimadzu QP-2010 SE GCMS)  
150 and thermal adsorption equipment (ENTECH 7100A Preconcentrator) in accordance with the  
151 analytical procedure of the TO-15 method. The analysis column in GC/MS was a Chrompack DB-1  
152 capillary column with an inner diameter of 0.25 mm and a length of 60 m. In quantification of VOC  
153 species, 101 standard curves were prepared using the standard gases adopted in the calibration  
154 mixture of the TO-14A method of the US EPA, the ozone precursor mixtures adopted in the TO-15  
155 method. Because these standard curves did not encompass all the compounds in the air samples, a  
156 semiquantitative method of analysis was used in which the analyte quantity was based on the standard  
157 curve of toluene (in the unit of parts per billion of toluene). Finally, all VOC concentrations were  
158 converted to the unit of parts per billion of carbon (ppbC). Because Tedlar bags are not as suitable as  
159 canisters for storing samples over long periods (more than approximately 30 days), the collected  
160 samples were analyzed within 10 days after sampling.

#### 161 2.5 Field measurements

162 We used the developed UAV platform for detecting air pollutant concentrations in a large special  
163 industrial zone that included a traditional industrial park, a precision machinery park, and a municipal  
164 waste incineration plant. Figure 4 shows the location of the study area, which is located at the southern  
165 piedmont of the Dadu Tableland in the western part of the Taichung Basin, Taiwan. Two industrial  
166 parks [the Taichung Industrial Park (TIP) and the Taichung Precision Machinery Park (TPMP)], a  
167 municipal waste incineration plant [the Wenshan Waste Incineration Plant (WWIP)], and a landfill  
168 (the Wenshan Landfill) were located within the study area. The TIP is a large industrial space with a  
169 total area of 5.82 km<sup>2</sup>. Currently, 1086 factories that employ a total of approximately 44 000 people

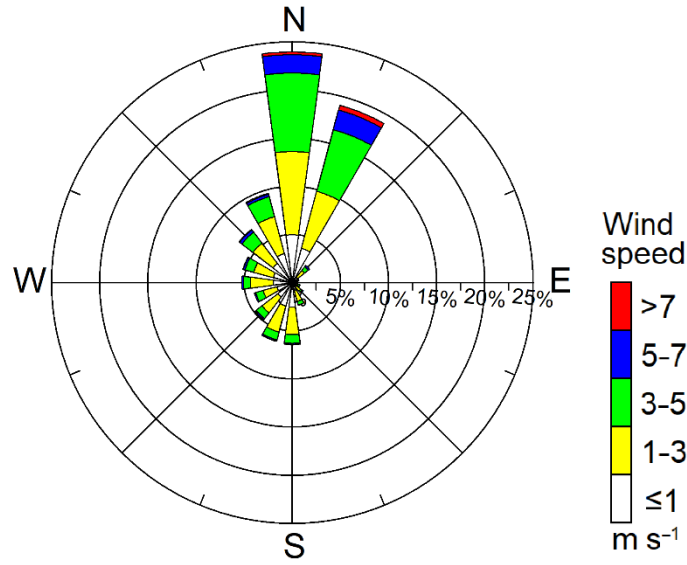
170 are located in this industrial park. In addition to traditional industries, high-tech industries, such as  
 171 optoelectronics, electronics, and precision machinery industries, are located in TIP. TPMP is an  
 172 industrial park with an area of 1.61 km<sup>2</sup> and mainly includes companies focusing on precision  
 173 machinery innovation. This industrial park is a crucial base of production of Taiwan's machinery  
 174 industry and has a land sales rate of 100%. As of the end of December 2022, 170 manufacturers that  
 175 employ approximately 21 329 people operate in TPMP. WWIP began operation in 1995 and was the  
 176 first large-scale incineration plant to be established in central Taiwan. This plant covers an area of  
 177 0.044 km<sup>2</sup> and has three incinerators that handle a total of 900 tons of waste per day. The Wenshan  
 178 Landfill was opened in 1983 and covers an area of 0.365 km<sup>2</sup>. The restoration of this landfill was  
 179 completed in March 2019 and involved the installation of a solar photovoltaic system with a capacity  
 180 of approximately 6.2 MWp on an area covering 0.0483 km<sup>2</sup>. In addition, a busy national freeway and  
 181 provincial expressway were located in the eastern part of the study area (Fig. 4) with weekday  
 182 southbound and northbound traffic volumes of approximately 112 150 and 85 480 PCU, respectively.



183  
 184 **Figure 4.** Locations of field measurement sites and Wenshan air quality monitoring station in the  
 185 case study area.

186 The annual prevailing wind directions in the study area are north and north–northeast, which can  
 187 be attributed to the spoon-shaped topography of the Dadu Tableland (Fig. 5). Moreover, the most  
 188 prevalent local average wind speed is 1–3 m s<sup>-1</sup>, followed by 3–5 m s<sup>-1</sup>. Therefore, three locations  
 189 were selected as field measurement sites (sites 1, 2, and 3) according to the prevailing wind directions  
 190 (Fig. 5). These sites were located in densely populated parts of the study area. Site 1 was located  
 191 upwind of the two industrial areas and WWIP, whereas sites 2 and 3 were located downwind of these  
 192 areas and WMWIP. Because of regulations limiting the altitude of local flights to 200 ft (61 m), the  
 193 heights at which samples were gathered were 2, 20, 40, and 60 m above the ground at each site. Noori  
 194 and Dahnil (2020) indicated that a UAV monitoring system can accurately measure the concentrations  
 195 of air pollutants at flight speeds slower than 6 m s<sup>-1</sup> and that detection accuracy decreases  
 196 considerably at flight speeds greater than 8 m s<sup>-1</sup>. Therefore, the flight speed of the developed UAV

197 platform was controlled at  $\leq 6 \text{ m s}^{-1}$  in this study.



198  
199 **Figure 5.** Annual wind rose of 2022 at the Wenshan air quality monitoring station.

## 200 2.6 Measurement of the speed and direction of the upper winds

201 To avoid the airflow caused by the rotor of the UAV from affecting the measurement of the speed  
202 and direction of the upper winds, the single-theodolite method was used in this study. A theodolite  
203 (WORLD E105-S Theodolite) was used to measure the speed and direction of the upper winds  
204 according to the pilot-balloon observation method (Pollak and Brunt, 1939). Figure 6 shows a  
205 schematic of the measurement of the upper winds by using the single-theodolite method, with Figs.  
206 6(a) and 6(b) displaying the ground-projection-based and sliding-rule-based wind field diagrams,  
207 respectively. The formula for computing the speed of the upper winds is as follows:

$$208 \quad u = 72L^{0.63}/(L + W)^{0.42} \quad (1)$$

$$209 \quad r_1 = Z_1 \cot H_1 \quad (2)$$

$$210 \quad V_e = Z_2 \cot H_2 \sin A_2 - Z_1 \cot H_1 \sin A_1 \quad (3)$$

$$211 \quad V_n = Z_2 \cot H_2 \cos A_2 - Z_1 \cot H_1 \cos A_1 \quad (4)$$

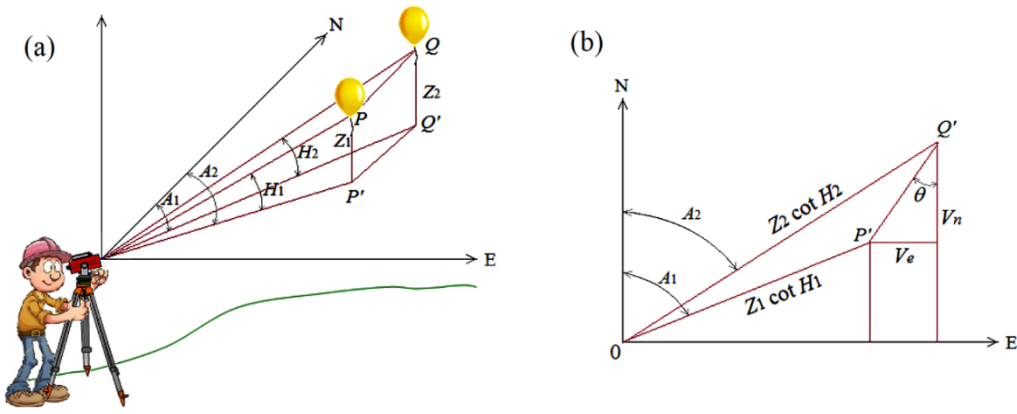
$$212 \quad \theta = \tan^{-1}(V_e/V_n) \quad (5)$$

$$213 \quad P'Q' = V_e / \sin \theta \quad (6)$$

$$214 \quad V = P'Q' / t \quad (7)$$

215 where  $u$ ,  $L$ , and  $W$  are the rising speed (m/s), buoyancy (g), and weight of the pilot balloon (g),  
216 respectively;  $r_1$ ,  $Z_1$ , and  $H_1$  are the projected length (m) from the ground up to point  $p$ , the rising  
217 height (m), and the elevation angle ( $^\circ$ ), respectively;  $V_e$  and  $V_n$  are the eastern and northern projection  
218 lengths (m) of the wind speed, respectively;  $\theta$ ,  $A_i$ , and  $V$  are the northeastern wind speed angle ( $^\circ$ ),  
219 azimuth angle ( $^\circ$ ), and average wind speed at time  $t$ , respectively; and  $P'Q'$  is  $PQ$  at ground projection  
220 (m). The wind directions at  $P'Q'$  in quadrants I, II, III, and IV are defined to be  $180^\circ + \theta$ ,  $180^\circ - \theta$ ,  $\theta$ ,  
221 and  $360^\circ - \theta$ , respectively.





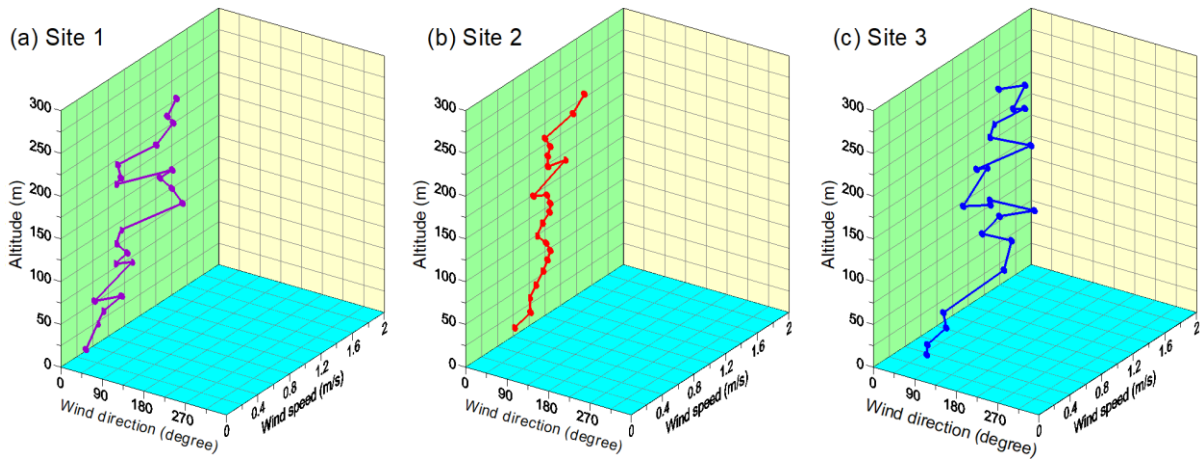
222  
223 **Figure 6.** (a) geometry of the single-theodolite method and (b) the slide-rule method of computation.

224 **3 Results and discussion**

225 3.1 Field measurement 1

226 3.1.1 Upper winds

227 **Figure 7** illustrates the observation results for the upper winds at the three field measurement  
 228 sites between 13:30 and 16:30 on 29 March 2023. During the observation period, all wind directions  
 229 at the three sites were between the north and northeast. All upper wind speeds observed at the three  
 230 sites were less than  $2 \text{ m s}^{-1}$ . The prevailing wind directions at sites 1, 2, and 3 were north–northeast,  
 231 north by east, and northeast, respectively. The wind speed at site 3 on the southern (downwind) side  
 232 was marginally higher than those at the other two sites. The wind speeds at the three sites increased  
 233 with altitude, which is consistent with the power law of the vertical distribution of wind speed. In the  
 234 Taichung Basin, the average hourly wind speed was mostly between 0 and  $3 \text{ m s}^{-1}$ . The sampling  
 235 period coincided with a period of comfortable weather in Taiwan.

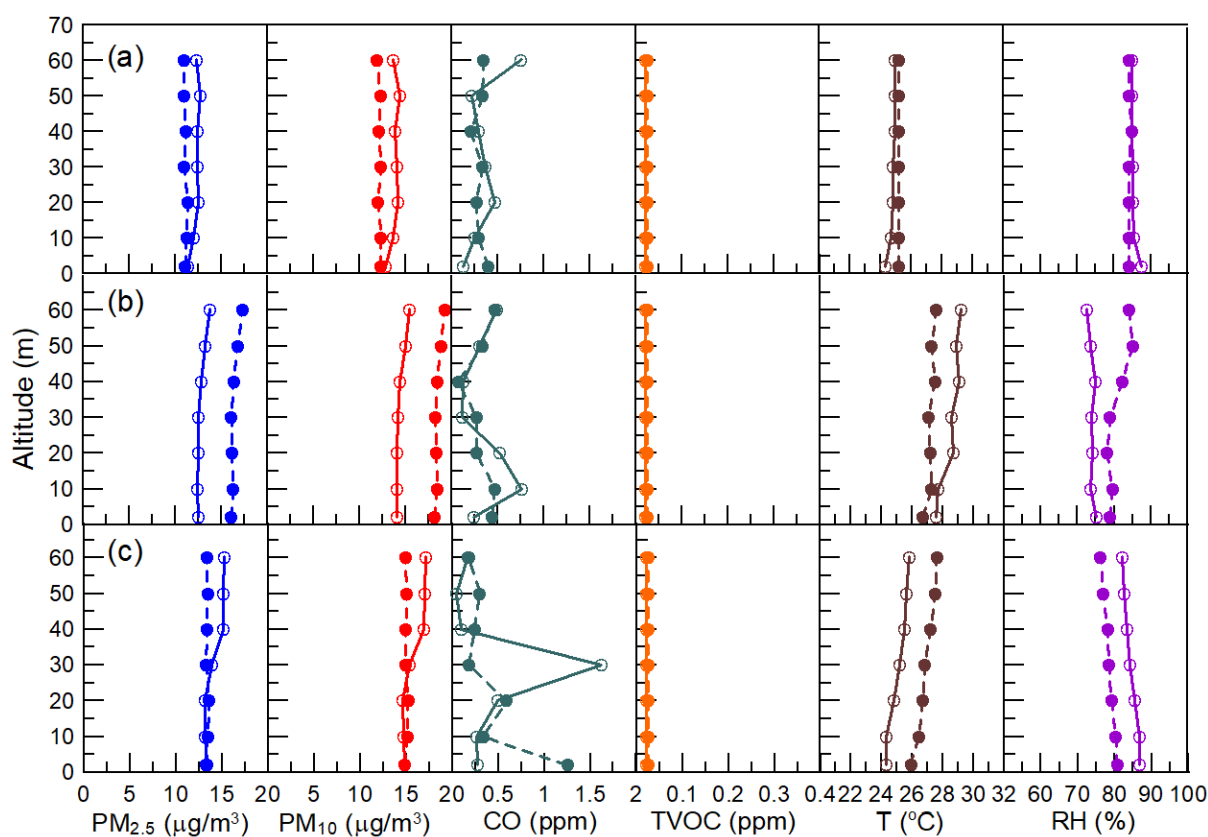


236  
237 **Figure 7.** The observation results of upper winds during 13:30–16:30 on 29 March 2023, (a)–(c) are  
 238 at sites 1–3, respectively.

239 3.1.2 Vertical distributions of critical air pollutants

240 Prior to each UAV telemetry run, the sensing system was connected to the IoT system to ensure  
 241 that the monitoring data were input to the cloud server. Two runs were conducted at each monitoring  
 242 site; thus, six runs were performed in total. Figure 7 displays the vertical distributions of critical air

243 pollutants, ambient temperature, and RH during 13:30–16:30 on 29 March 2023. In Fig. 8, the solid  
 244 and dashed lines represent the results obtained in runs 1 and 2 at each site, respectively. The PM<sub>2.5</sub>  
 245 and PM<sub>10</sub> concentrations at the three sites were 11.0–17.3 (average = 13.4) and 11.9–19.3 (average =  
 246 15.0), respectively. The highest and lowest concentrations of PM (both PM<sub>2.5</sub> and PM<sub>10</sub>) were  
 247 observed at sites 2 (downwind) and 1 (upwind), respectively. The results indicate that the investigated  
 248 industrial zone had high local PM concentrations, especially at site 2. CO is mainly emitted from  
 249 mobile sources. Although the CO concentrations at the three sites were marginally variable but low.  
 250 Therefore, the differences in the influences of the mobile source on the three locations were small.  
 251 The TVOC concentrations at the three sites were very low ( $\leq 0.02$  ppm), which might be attributable  
 252 to the lack of large VOC emission sources in the investigated industrial zone. Because the sensitivities  
 253 of the O<sub>3</sub> and NO<sub>2</sub> sensors were too low (Table 1), their monitoring data were 0 ppm in all the  
 254 measurements.

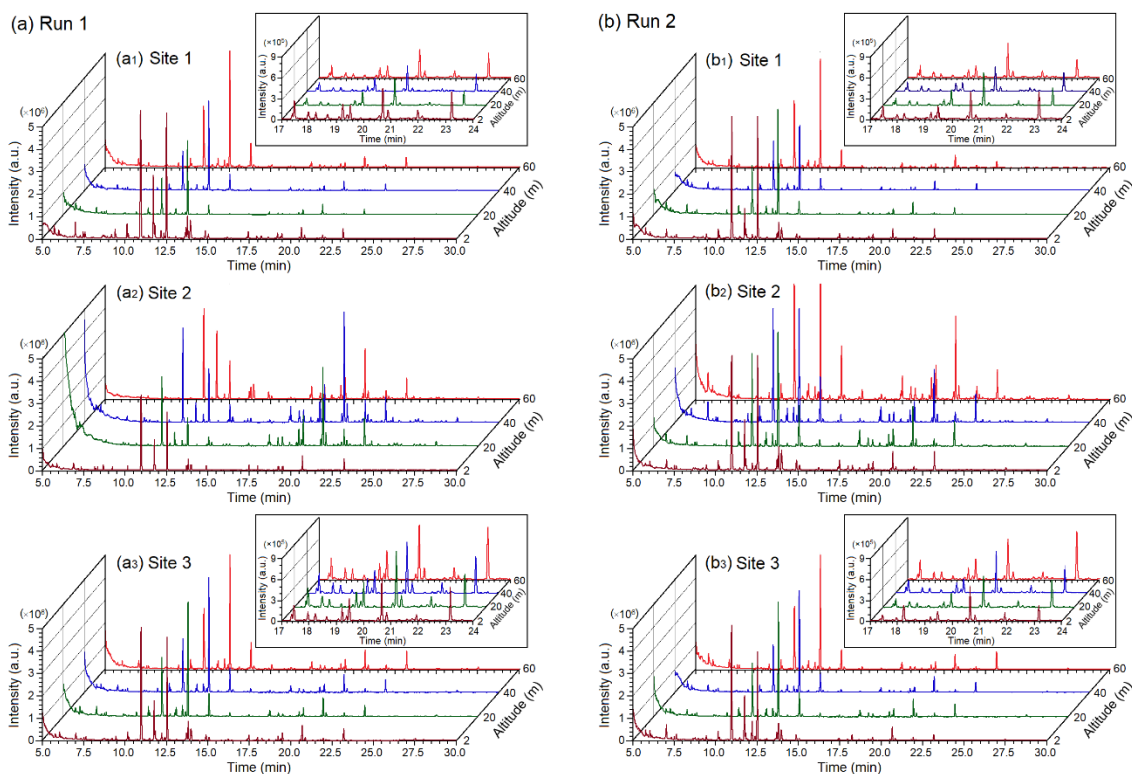


255  
 256 **Figure 8.** The observation results of critical air pollutants, ambient temperature, and relative humidity  
 257 during 13:30–16:30 on 29 March 2023, (a)–(c) are at Sites 1–3, respectively. Solid and dashed lines  
 258 are the results of Run 1 and Run 2, respectively.

259 The temperature ranges at sites 1 to 3 were 24.3–25.2 °C (average = 25.0 °C), 26.7–29.2 °C  
 260 (average = 27.9 °C), and 24.3–27.6 °C (average = 26.0 °C). At all locations, the lowest temperature  
 261 was observed at the ground because of the heat radiation from the surface on cloudy days. The  
 262 temperatures at the three sites gradually decreased in the afternoon with time. The RH values of the  
 263 three locations changed with the temperature, and the RH range in the study area was 76.1%–87.6%.

264 3.2.3 Vertical distributions of VOCs

265 Sampling was performed twice at four altitudes at each site by using the UAV platform; thus,  
266 eight samples were collected per site. Figure 9 displays the analysis results obtained through GC-MS  
267 with thermal adsorption equipment for the upper-altitude VOCs at the three sites during 13:30–16:30  
268 on 29 March 2023, using GC-MS. A total number of more than 56 species were analyzed at different  
269 altitudes at the each site. The analysis results indicated the feasibility of using the developed UAV  
270 platform with a Tedlar bag sampling system for the 3D measurement of VOC concentrations in  
271 accordance with the TO-15 method. All dominant VOCs at various altitudes at the three sites appeared  
272 within the retention time of 10–15 min in GC-MS chromatography. The peak patterns of the dominant  
273 species at the three sites were highly similar, which indicated that the three sites had similar air  
274 pollution sources. A second set of dominant VOCs appeared at various altitudes within the retention  
275 time of 17–24 min, especially at site 3. The second dominant species at site 2 had a considerably  
276 higher concentration than did those at the other sites, which indicated that site 2 was located  
277 downwind of some air-pollution emission sources. TIP is located upwind of site 2 (Fig. 4).



278

279 Fig. 9. The analysis results of upper-altitude VOCs during 13:30–16:30 on 29 March 2023. (a) and  
280 (b) show the results of run 1 and run 2, respectively. The insets in each subfigure are zoomed-in views  
281 over the retention time range from 17 to 24 minutes.

282 Table 2 lists the qualitative and quantitative analysis results of the VOC samples collected from  
283 the three sites, where the concentration is the average of those obtained in two sampling runs (runs 1  
284 and 2 in Fig. 9). The concentrations of the top five VOC species at the four sampled altitudes had the  
285 following order from highest to lowest: site 1, toluene > 2,4-dimethyl heptane > 4-methyl octane >  
286 propyl propionate > 3,7-dimethyl undecane; site 2, 2,4-dimethyl heptane > toluene > 4-methyl octane

287 > 3,7-dimethyl undecane > propyl propionate; and site 3, 2,4-dimethyl heptane > toluene > 4-methyl  
 288 octane > propyl propionate > 3,7-dimethyl undecane. The ranges of the concentration ratio of the top  
 289 five species to all upper-altitude VOCs at sites 1, 2, and 3 were 71.1%–80.9% (average = 74.9%),  
 290 69.1%–79.7% (average = 72.9%), and 72.3%–76.8% (average = 73.6%), respectively. Thus, the top  
 291 five VOC species dominated the upper-altitude VOC concentrations.

292 **Table 2.** The average concentrations (in ppbC) of upper-altitude VOCs at the three sites during March 29, 2023.

Species	Retention time (min)	Altitude at Site 1 (m)				Altitude at Site 2 (m)				Altitude at Site 3 (m)			
		2	20	40	60	2	20	40	60	2	20	40	60
Ethanol	5.70	1.8	2.3	1.4	1.2	0.6	2.9		5.1	1.7	1.2	1.7	2.0
Acetone	5.98	0.8	0.8	0.8	0.6	0.9	0.8	1.4	1.2	1.4	1.2	0.8	0.9
Isopropanol	6.11	0.6	0.9							0.6			
2-Methyl pentane	6.99	3.9	3.5	2.6	3.0	3.3	4.7	9.0	4.8	5.1	4.4	2.7	3.6
2-Butanone	7.29	0.3	0.3	0.3	0.3	0.2	0.2	0.3	0.2	0.3	0.3	0.3	0.3
Hexane	7.48	1.4	0.6	0.6	0.6	1.4	1.1	1.2	0.9	0.8	0.9	0.6	1.2
Ethyl Acetate	7.58	1.1	0.8	0.8	0.8	0.8	0.9	0.8	0.9	1.1	0.8	0.8	0.8
Benzene	8.59		0.2	0.2	0.2	0.5	0.8	0.9	1.1	0.3	0.5	0.5	0.3
1-Butanol	8.62	0.5			0.2					0.2			
2-Methyl hexane	8.73	0.3	0.5	0.3	0.2		0.3	0.5	0.5	0.2	0.3	0.3	0.3
Cyclohexane	8.91	0.5											
3-Methyl hexane	8.95	0.3	0.2	0.2	0.2	0.3	0.3	0.5	0.5	0.5		0.3	0.3
Pentanal	9.07	0.2	0.0	0.0	0.0					0.2		0.0	0.2
1,2-Dichloro propane	9.19	1.2				0.5				0.8			
Heptane	9.40	1.7	1.1	0.9	1.1	1.8	1.8	2.6	2.0	1.2	1.2	1.1	1.2
2,5-Dimethyl hexane	10.12	3.5	2.1	1.7	2.4	2.7	4.2	5.0	4.4	2.4	2.7	2.3	2.7
2,4-Dimethyl hexane	10.19	0.8	0.5	0.5	0.8	0.8	1.1	1.4	1.4	0.8	0.8	0.6	0.8
2,5-Dimethyl-1-hexene	10.58	0.2	0.0	0.0	0.0			0.2	0.0	0.0	0.0	0.0	0.0
2-Ethyl-1-butanol	10.70	0.5	0.3	0.3	0.5		0.5	0.5	0.5	0.3	0.5	0.3	0.5
Toluene	10.94	87.9	16.5	17.3	25.1	71.3	35.7	45.5	45.2	49.2	23.0	19.7	24.5
3-Methyl heptane	11.15	0.3	0.2	0.2	0.2		0.5	0.3	0.3	0.3	0.2	0.2	0.3
Hexanal	11.44	0.5	0.3	0.3	0.5	0.5	0.5	0.5	0.6	0.5	0.5	0.5	0.5
Propyl propionate	11.71	15.6	0.3	0.3	0.9	17.1	1.2	1.5	2.3	13.7	0.6	0.5	0.9
Octane	11.79	3.5	1.8	1.4	2.0	2.1	3.5	3.5	3.9	1.1	2.0	1.7	2.1
2,3,5-Trimethyl hexane	12.36	1.2	0.8	0.8	0.9	1.2	1.7	2.0	2.3	1.1	1.4	1.1	1.1
2,4-Dimethyl heptane	12.50	42.9	28.1	24.6	41.3	43.8	62.4	77.4	81.6	30.5	38.6	35.3	42.2
2,6-Dimethyl heptane	12.66	0.3	0.2	0.2	0.2	0.3		0.3	0.5		0.2	0.2	0.2
2,4-Dimethyl-1-heptene	13.06	0.2	0.2	0.2	0.2	0.3	0.3	0.3	0.3	0.2	0.2	0.2	0.2
3-Ethyl-2-methyl hexane	13.60	0.2	0.0	0.2	0.2		0.5	0.5	0.6	0.2	0.3	0.3	0.3
Ethyl benzene	13.68	3.0	0.0	0.2	0.2	3.9				2.4		0.3	0.3
4-Methyl octane	13.77	6.5	3.8	4.7	6.9	7.8	13.4	15.6	17.7	5.7	6.9	6.9	8.0
m-Xylene	13.94	10.4	0.5	0.6	1.2	14.7	2.3	2.1	2.9	7.8	0.9	1.2	1.5
o-Xylene	14.84	3.3		0.3	0.6	6.6	0.9	0.9	1.4	3.5	0.6	0.5	0.3
Nonane	15.03	1.1	0.5	0.6	0.8	1.5	2.0	2.7	3.2	0.8	1.1	1.1	1.2
2,4,6-trimethyl heptane	15.80							0.2	0.3				0.2
3,5-Dimethyl octane	16.04	0.2		0.0	0.2		0.3	0.3	0.5		0.2		0.2
2,7-Dimethyl octane	16.18	0.3	0.2	0.2	0.3	0.8	1.1	1.2	1.4	0.5	0.5	0.5	0.5
2,6-Dimethyl octane	16.40	0.2					0.3	0.5	0.5		0.2		0.2
2,5-Dimethyl octane	17.36	0.3	0.2	0.2	0.3	0.6	1.2	1.1	1.7	0.3	0.3	0.3	0.5
2-Methyl nonane	17.44	1.5	0.6	0.8	1.2	2.4	4.2	3.9	5.9	0.9	1.2	1.4	1.8
2,5-Dimethyl nonane	17.95	0.6	0.5	0.5	0.6	1.2	2.4	2.6	3.8	0.6	0.9	0.9	0.9
Decane	18.64	0.3	0.2	0.2	0.3	0.6	1.1	0.9	1.4	0.3	0.3	0.3	0.5
4-Methyl decane	19.07	0.2	0.2	0.2	0.2	0.2	0.5	0.8	1.2	0.2	0.2	0.2	0.2
Undecane	19.20	0.9	0.5	0.6	0.8	1.7	3.2	3.0	5.7	0.8	0.9	1.1	1.2
2,5,6-Trimethyl decane	19.36	0.3	0.2	0.2	0.2	0.3	0.9	0.8	1.5	0.3	0.3	0.3	0.3
4-Methyl-5-propyl nonane	19.47	1.1	1.1	0.8	0.9	1.8	3.9	4.7	7.5	1.2	1.5	1.4	2.0
Dodecane	20.53	0.3	0.2	0.2	0.2	0.3	0.8	1.2	1.7	0.3	0.3	0.3	0.5
3,7-Dimethyl undecane	20.65	2.4	2.6	2.1	2.6	4.4	9.2	12.8	19.1	3.2	3.5	3.8	3.9
4-Methyl-1-undecene	20.84	0.2	0.0	0.2	0.2	0.2	0.5	0.5	0.9	0.2	0.2	0.2	0.2
Undecanal	21.56			0.2			0.3	0.3	0.5			0.2	0.2
2,3-Dimethyl decane	21.77		0.2	0.2	0.2		0.5	0.6	0.9	0.2	0.2	0.2	0.2
Tridecane	21.93	0.5	0.3	0.2	0.5	0.8	1.5	2.1	2.7	0.5	0.6	0.6	0.8
2,3,5,8-Tetramethyl decane	22.09	0.2	0.0	0.2	0.2		0.5	0.6	0.9	0.2	0.2	0.2	0.2
2-Heptyl-1,3-dioxolane	22.27			1.5	1.5								
2-Methyl tridecane	23.59						0.3	0.5	0.6				0.0
2,6-Dimethyl undecane	24.00						0.2		0.5				
Total		204.8	72.9	69.5	102.3	199.5	176.1	214.8	244.2	143.3	101.7	92.6	111.9

293 Toluene and 2,4-dimethyl heptane exhibited the highest or second-highest concentrations among  
 294 the VOCs at the three sites. Toluene might originate from vehicle exhaust and industrial emissions.

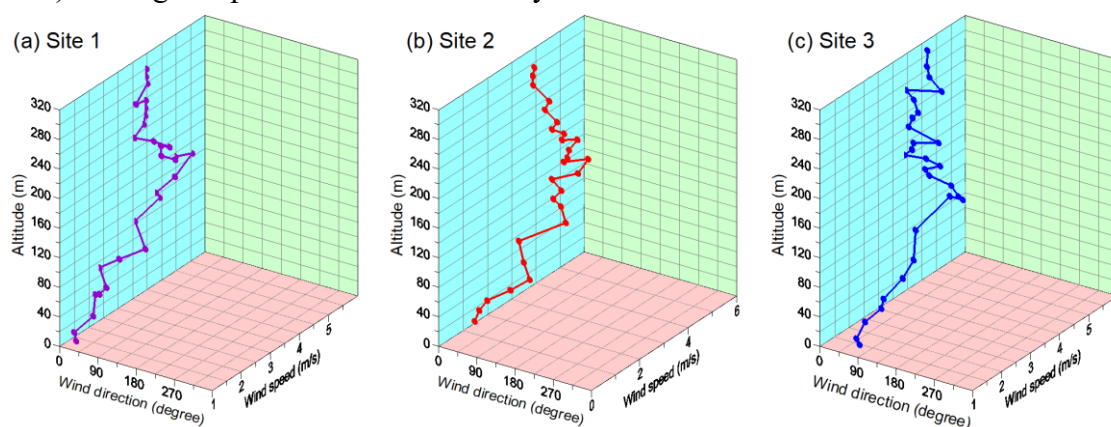


295 Common industrial organic solvents, such as benzene, xylene, ethylbenzene, and butanone, were  
296 detected at the four altitudes at each site, which indicated that a considerable quantity of the toluene  
297 in the study area originated from industrial emissions. In general, because its branched structure  
298 allows for combustion without knocking, 2,4-dimethyl heptane is blended with other gasoline  
299 components to produce high-octane fuel. In addition, alkanes were the dominant VOC species at  
300 various altitudes and sites. Thus, the concentrations of the VOCs originating from vehicle exhaust  
301 might have been higher than those of the VOCs originating from industrial exhaust. Propyl propionate  
302 is a safer alternative for toluene because of its low odor, moderately volatile nature, and nonhazardous  
303 and nonpolluting ester product; thus, the propyl propionate detected field measurement 1 mainly  
304 originated from industrial emissions. The average VOC concentrations at the three sites had the  
305 following order from highest to lowest: site 2 > (site 1  $\approx$  site 3). The highest and second-highest total  
306 VOC concentrations at sites 1 and 3 appeared at altitudes of 2 and 60 m, respectively. By contrast,  
307 the highest and second-highest total VOC concentrations at site 2 appeared at altitudes of 60 and 40  
308 m, respectively. This result indicates that some VOCs were transmitted from upwind sources.

## 309 3.2 Field measurement 2

### 310 3.2.1 Upper winds

311 **Figure 10** shows the observation results for the upper winds at the three field measurement sites  
312 between 13:30 and 16:30 on 10 May 2023. During the measurement period, all wind directions at the  
313 three sites were between north and east. The prevailing wind directions at sites 1, 2, and 3 were north-  
314 northeast, northeast by east, and northeast by east, respectively. The upper wind speeds at sites 1-3  
315 were 1.1-5.6 m s<sup>-1</sup> (average = 3.5 m s<sup>-1</sup>), 1.2-5.1 m s<sup>-1</sup> (average = 3.6 m s<sup>-1</sup>), and 1.2-5.2 m s<sup>-1</sup>  
316 (average = 3.7 m s<sup>-1</sup>), respectively. The wind speeds at the three sites increased with an increase in  
317 altitude but decreased marginally as the altitude increased beyond 200 m. Compared with the upper  
318 winds during the field measurement 1 (on 29 March 2023), those during field measurement 2 (on 10  
319 May 2023) had higher speed and a more easterly direction.

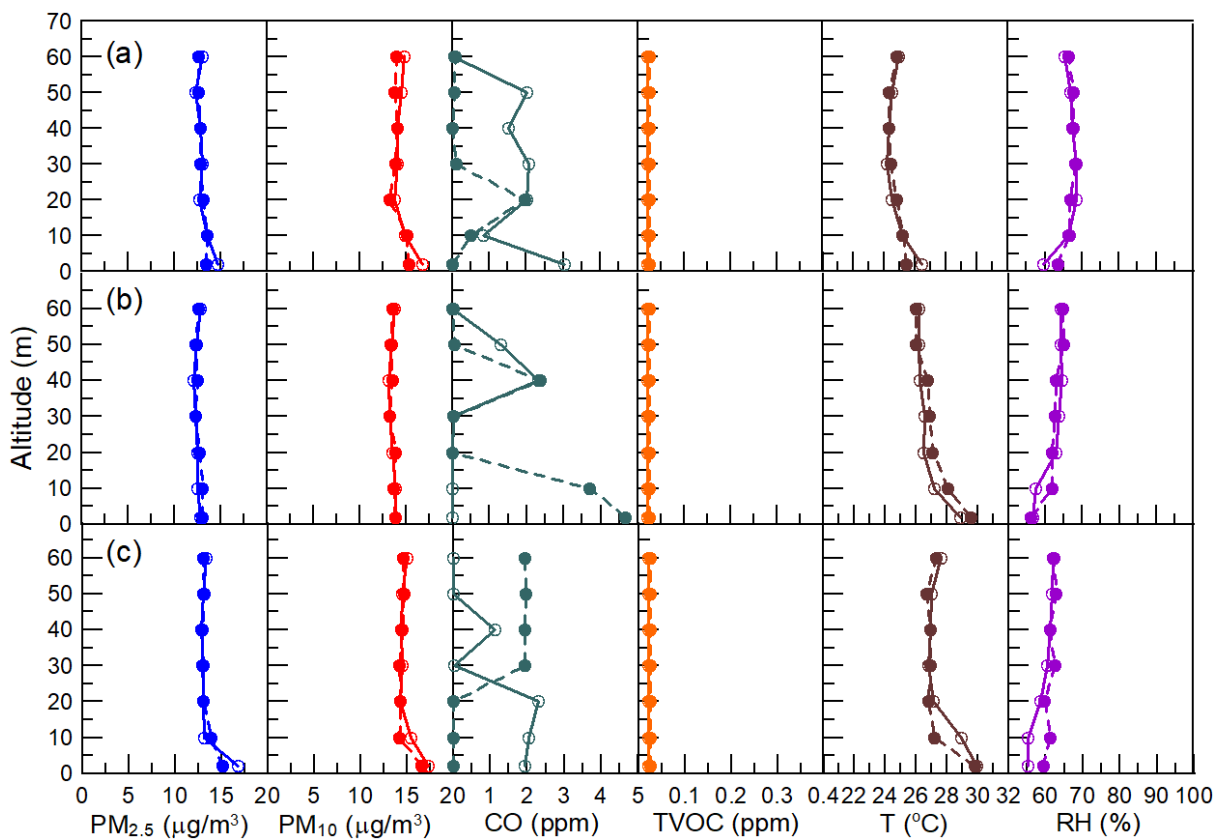


320  
321 **Figure 10.** The observation results of upper winds during 13:30-16:30 on 10 May 2023.

### 322 3.2.2 Vertical distributions of critical air pollutants

323 As was the case in field measurement 1, two runs of UAV telemetry were implemented at each  
324 monitoring site; thus, a total of six runs were performed. The sensing system was connected to the

325 IoT system prior to UAV telemetry to ensure that the monitoring data were input to the cloud server  
 326 after each run. **Figure 11** displays the vertical distributions of critical air pollutants, ambient  
 327 temperature, and RH for the period of 13:30–16:30, 10 May 2023. The PM<sub>2.5</sub> and PM<sub>10</sub> concentration  
 328 ranges at the three sites were 12.1–16.8 μg m<sup>-3</sup> (average = 13.1 μg m<sup>-3</sup>) and 13.1–17.4 μg m<sup>-3</sup>  
 329 (average = 14.3 μg m<sup>-3</sup>), respectively. The highest and lowest concentrations of PM (both PM<sub>2.5</sub> and  
 330 PM<sub>10</sub>) were observed at sites 3 (downwind) and 2 (upwind), respectively. The highest CO  
 331 concentrations at the three sites **were** at the ground level, and the highest CO concentration of 4.66  
 332 ppm was measured at site 2. The CO concentrations at all altitudes except for the ground level at the  
 333 three sites varied between 0 and 2.4 ppm. As was the case in field measurement 1, the O<sub>3</sub> and NO<sub>2</sub>  
 334 concentrations were 0 ppm in measurement 2 because the sensitivities of the O<sub>3</sub> and NO<sub>2</sub> sensors  
 335 were too low. The TVOC concentrations at the three sites were very low (≤0.02 ppm; as in field  
 336 measurement 1), possibly because the sensitivity of the TVOC sensor was too low.

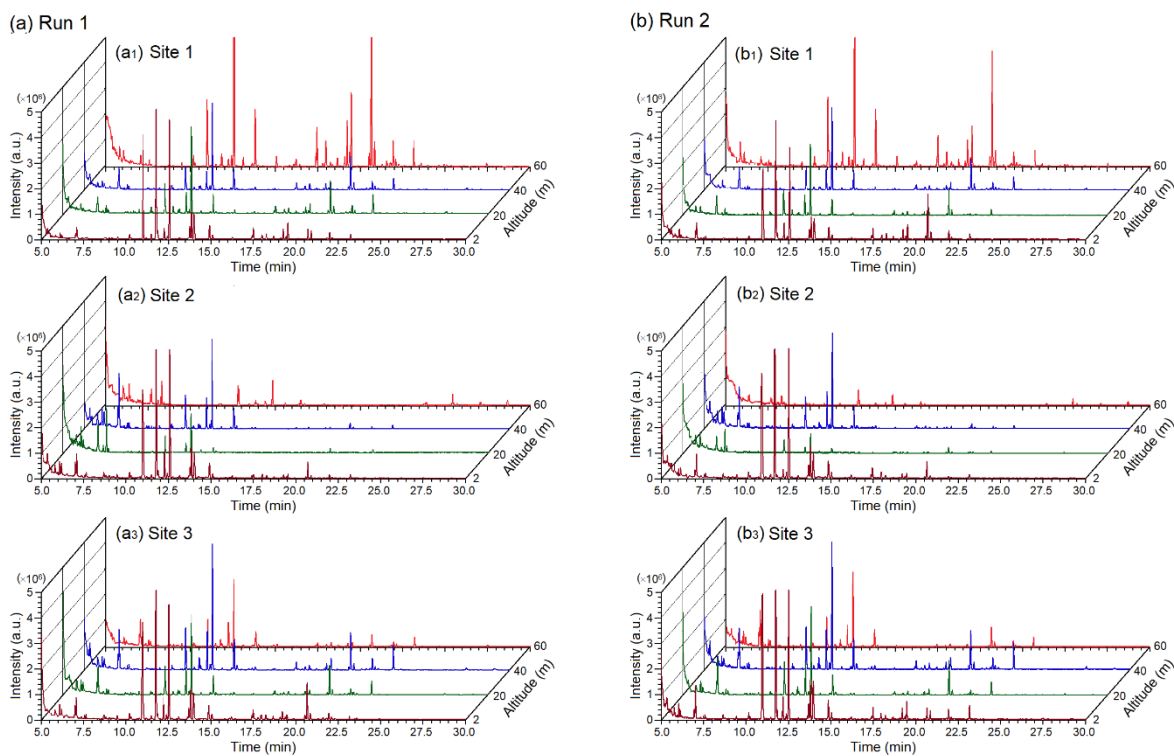


337 **Figure 11.** The observation results of critical air pollutants, ambient temperature, and relative  
 338 humidity during 13:30–16:30 on 10 May 2023, (a)–(c) are at sites 1–3, respectively. Solid and dashed  
 339 lines are the results of run 1 and run 2, respectively.  
 340

341 The temperature ranges at sites 1–3 were 24.12–26.4 °C (average = 24.9°C), 26.0–29.6 °C  
 342 (average = 27.0 °C), and 26.7–29.9 °C (average = 27.6 °C), respectively. The highest temperatures at  
 343 these sites were observed at the ground level because of the thermal radiation of the surface on sunny  
 344 days. The temperatures at the three sites gradually decreased in the afternoon with time. The RH  
 345 values of the three sites changed with the temperature, and the RH range in the study area was 55.1%–  
 346 68.4%.

347 3.2.3 Vertical distributions of VOCs

348 **Figure 12** depicts the GC–MS analysis results for upper-altitude VOCs at the three field  
349 measurement sites during 13:30–16:30 on 10 May 2023. Sampling was performed twice at four  
350 altitudes (2, 20, 40, and 60 m) at each site by using the UAV platform; thus, a total of 24 measurements  
351 were performed (eight at each site). A total of 79 VOCs species were analyzed at different altitudes  
352 at the three sites, and this number is higher than the number of VOCs analyzed in field measurement  
353 1 (i.e., 52). All the dominant VOC species at various altitudes at the three sites appeared within the  
354 retention time of 10–15 min in GC–MS chromatogram, which is **in line** with the results obtained in  
355 field measurement 1. The peak patterns of the dominant VOC species at the three sites were highly  
356 similar, which indicated that the three sites had similar air pollution sources. The highest peak  
357 intensities of the dominant VOC species at the three locations were observed at an altitude of 2 m. A  
358 second dominant VOC species appeared at various altitudes within the retention time of 17–24 min,  
359 especially at an altitude of 60 m at site 1. The peak intensity of the second dominant species at site 2  
360 was considerably lower than those at the other two sites. In addition, the concentrations of all the  
361 VOCs at an altitude of 60 m at site 2 were lower than those at the same altitude at sites 1 and 3.



362 **Figure 12.** The analysis results of upper-altitude VOCs during 13:30–16:30 on 10 May 2023. (a) and  
363 (b) show the results of run 1 and run 2, respectively.

365 Table 3 lists the average upper-altitude VOC concentrations at the three sites on 10 May 2023.  
366 The total upper-altitude VOC concentrations at the three sites in field measurement 2 was marginally  
367 lower than that in field measurement 1; however, the total number of VOC's detected in field  
368 measurement 2 was higher than that in field measurement 1. In addition, the highest and lowest VOC  
369 concentrations occurred at an altitude of 2 m at site 3 and at an altitude of 60 m at site 1, respectively.  
370 This result is different to that obtained in field measurement 1.

**Table 3.** The average concentrations (in ppbC) of upper-altitude VOCs at the three sites during May 10, 2023.

Species	Retention time (min)	Altitude at Site 1 (m)				Altitude at Site 2 (m)				Altitude at Site 3 (m)			
		2	20	40	60	2	20	40	60	2	20	40	60
1-Butene	5.27	2.0	4.6	4.9		4.0	2.6	4.7	0.2	3.5	3.2	3.8	2.8
Ethylene oxide	5.58	2.1	1.4			2.2	2.7	2.6	2.2	2.2	1.6	0.7	0.3
Ethanol	5.73	0.7	1.0	1.4	2.5	1.7	2.1	3.8	1.8	2.7	3.5	2.9	1.9
Acetone	6.00	1.0	1.1	1.6	0.6	1.8	2.2	3.1	1.6	2.6	2.7	1.7	1.7
Isopropanol	6.11	0.8	0.9	1.1		3.1	1.3	5.8	0.6	1.9	4.2	3.1	1.9
Cyclobutanol	6.39	0.3	0.6	0.5	0.3	1.1	0.6	0.9	0.5	0.8	0.4	0.4	0.4
2-methyl-2-Propanol	6.48				1.7								
trimethyl Silanol	6.93	1.7				4.7		4.2		3.1	2.5	3.7	1.7
2-Methyl pentane	6.99	5.9	9.0	11.0	3.0	7.7	6.1	14.2	3.3	9.4	9.7	15.3	12.5
2-Butanone	7.29	0.2	0.3	0.3	0.2	0.3	0.6	0.4	0.3	0.3	0.4	0.4	0.4
Hexane	7.47	0.6	2.2	1.3	1.2	1.0	7.7	1.6	4.0	1.2	1.9	1.6	1.9
Ethyl Acetate	7.58	0.5	0.5	0.6	0.4	1.0	0.7	1.2	0.3	1.2	0.9	1.0	1.0
2-methyl-1-Propanol	7.92					0.2		0.3	0.1		0.2	0.2	0.1
Benzene	8.61		0.2			1.8	0.3	0.6	0.2	1.6	0.5	0.5	0.3
1-Butanol	8.66	0.6	0.2		0.4								
2-Methyl hexane	8.73	0.1	0.2		0.2	0.4	0.3	0.4	0.2	0.3	0.4	0.3	0.3
3-Methyl hexane	8.93	0.2	0.2		0.2	0.5	0.3	0.5	0.2	0.4	0.4	0.4	0.4
Pentanal	9.07	0.1	0.2		0.1	0.1	0.0	0.1		0.1	0.2	0.1	0.1
1-Heptene	9.13	0.1	0.1		0.0	0.1	0.0	0.1		0.1	0.1	0.1	0.1
2,2,4-trimethyl-Pentane	9.27				0.0	0.1	0.1		0.1				
Heptane	9.41	0.7	0.7	0.5	0.9	1.0	0.2	0.8	0.2	1.0	0.6	0.7	0.6
2,5-Dimethyl hexane	10.12	1.0	1.2	0.9	2.3	1.5	0.2	1.0	0.2	1.7	1.0	1.1	1.0
2,4-Dimethyl hexane	10.20	0.3	0.3	0.3	0.6	0.4	0.1	0.3	0.1	0.5	0.3	0.4	0.2
2-Ethyl-1-butanol	10.71	0.3	0.2		0.3	0.2	0.2	0.3		0.4	0.2	0.3	0.2
Toluene	10.94	41.0	9.4	8.0	18.7	52.3	3.7	11.0	4.1	55.9	10.0	12.9	9.7
3-Methyl heptane	11.14	0.2	0.1	0.1	0.2	0.2	0.1	0.2		0.3	0.2	0.2	0.2
Hexanal	11.42	0.6	1.1	0.4	0.4	0.6	0.2	0.4	0.1	0.4	0.5	0.5	0.5
Propyl propionate	11.71	50.6	0.5	0.6	0.3	74.4		1.4	0.6	64.9	1.1	2.7	1.7
Octane	11.80	0.8	0.7	0.6	2.5	1.0	0.1	0.7	0.1	1.2	0.7	0.6	0.4
Hexamethylcyclotrisiloxane	12.17	4.3	6.6	6.4	2.1	5.7	1.7	10.2	0.8	7.4	7.7	11.0	7.5
2,3,5-Trimethyl hexane	12.36	0.9	0.9	1.0	2.1	1.6	0.2	1.3	0.2	1.5	1.2	1.4	1.0
2,4-Dimethyl heptane	12.51	28.9	21.7	23.1	64.0	40.0	5.8	25.0	3.8	39.7	23.7	28.9	19.6
2,6-Dimethyl heptane	12.67	0.2	0.1		0.3	0.2		0.1		0.3	0.1	0.2	0.1
2,4-Dimethyl-1-heptene	13.06	0.2	0.2	0.2	0.6	0.2	0.1	0.1	0.1	0.2	0.2	0.2	0.1
3-Ethyl-2-methyl hexane	13.60	0.2	0.3	0.4	0.6	0.3	0.1	0.3	0.1	0.3	0.4	0.4	0.3
Ethylbenzene	13.67	3.3				3.4	0.1	0.2	0.2	4.4		0.4	0.2
4-Methyl octane	13.77	7.0	5.0	5.9	13.8	8.5	0.9	6.1	0.9	9.4	5.6	7.2	4.6
m-Xylene	13.94	14.7	0.7	0.7	0.5	15.6	0.3	1.6	0.5	20.3	1.0	2.5	1.0
3-ethyl-2,3-dimethyl Pentane	14.22	0.1	0.1		0.2	0.3	0.7	0.1				0.1	
1,3,5,7-Cyclooctatetraene	14.63	0.2	0.2		0.1	0.2	0.2	0.2				0.2	0.2
o-Xylene	14.84	7.5	0.3		0.3	8.8	0.2	0.5	0.5	9.5	0.5	1.1	0.5
Nonane	15.03	1.4	0.7	0.7	2.5	1.4	0.2	0.4	0.2	1.9	0.6	0.8	0.5
2,4,6-trimethyl heptane	15.78	0.1	0.0		0.2	0.1				0.1		0.1	
3,5-Dimethyl octane	16.05	0.2	0.1		0.5	0.3				0.3		0.1	
2,7-Dimethyl octane	16.18	0.6	0.3	0.3	1.6	0.7		0.2		0.8	0.2	0.3	0.2
2,6-Dimethyl octane	16.40	0.2	0.1		0.5	0.2				0.2		0.1	
2,5-Dimethyl octane	17.37	0.6	0.3	0.3	1.7	0.4		0.1		0.6	0.2	0.3	0.2
2-Methyl nonane	17.44	2.4	1.2	1.3	6.4	1.3	0.1	0.4	0.2	2.3	0.8	1.3	0.7
2,2,3,5-Tetramethyl heptane	17.53		0.2				0.1	0.1				0.2	0.1
6-Methyl-5-hepten-2-one	17.83		0.0	0.1	0.2		0.0	0.0	0.1	0.1	0.1	0.1	0.0
2,5-Dimethyl nonane	17.96	1.2	0.8	0.8	4.7	1.3	0.1	0.3	0.1	1.5	0.6	0.7	0.5
Octamethylcyclotetrasiloxane	18.21	1.4	0.9	1.0	0.7	0.5	0.1	0.2	0.1	0.9	0.6	0.9	0.7
Octanal	18.32	0.1	0.2	0.1	0.3							0.1	0.1
Decane	18.65	0.8	0.3	0.4	1.6	0.2		0.2	0.1	0.7	0.3	0.4	0.2
4-Methyl decane	19.07	0.4	0.2	0.2	1.5	0.1		0.1		0.4	0.2	0.2	0.1
Undecane	19.21	2.1	1.1	1.2	7.0	0.8	0.1	0.2	0.1	2.1	0.7	1.2	0.6
2,5,6-Trimethyl decane	19.37	0.7	0.3	0.2	2.0	0.2			0.1	0.6	0.2	0.3	0.2
4-Methyl-5-propyl nonane	19.47	3.1	1.6	1.6	9.7	0.8	0.1	0.3	0.3	2.2	1.2	1.7	0.8
2,3-Dimethyl decane	20.53	0.5	0.5	0.5	2.2	0.2	0.1	0.1	0.1	0.6	0.4	0.5	0.4
3,7-Dimethyl undecane	20.66	5.5	5.9	6.4	26.2	3.2	0.7	1.0	1.3	5.0	5.5	7.2	3.1
4-Methyl-1-undecene	20.85	0.4	0.3	0.4	1.0	0.1	0.0	0.1	0.1	0.4	0.3	0.4	0.2
7-Methyl-1-undecene	21.11	0.0	0.0	0.0	0.1	0.0				0.0	0.0	0.0	0.0
2-methyl-1-Decanol	21.30				0.5								
Undecanal	21.43	0.1	0.2	0.2	0.5					0.3	0.3	0.2	0.2
Dodecane	21.59	0.4	0.3	0.3	0.8	0.1		0.1		0.4	0.3	0.4	0.2
Tridecane	21.78	1.4	0.8	1.5	3.2	0.4	0.1	0.3	0.3	1.5	0.9	1.6	0.9
2,3,5,8-Tetramethyl decane	22.09	0.4	0.3	0.5	0.9	0.1	0.0	0.1	0.2	0.4	0.3	0.5	0.3
4-Methyl tridecane	22.27	0.2	0.2	0.2	0.3	0.1				0.2	0.2	0.2	0.1
Tetramethylsilane	23.16	3.7	8.3	7.8	12.4	2.4	1.1	2.0	2.2	5.8	8.7	12.6	6.4
4-methyl Undecane	23.48	0.1	0.1		0.2					0.1		0.1	
2-Methyl tridecane	23.60	0.1	0.0	0.1	0.4	0.0				0.2		0.1	0.0
2,6-Dimethyl undecane	24.00	0.1	0.1		0.3					0.1			
Total		208.3	98.1	97.7	211.8	263.2	45.7	112.3	33.7	280.1	110.6	141.8	94.5



372 The top five VOCs at the four altitudes had the following order from highest to lowest: site 1,  
373 2,4-dimethyl heptane > toluene > propyl propionate > 3,7-dimethyl undecane > tetramethylsilane;  
374 site 2, propyl propionate > 2,4-dimethyl heptane > toluene > 2-methyl pentane >  
375 hexamethylcyclotrisiloxane; and site 3, 2,4-dimethyl heptane > toluene > propyl propionate > 2-  
376 methyl pentane > tetramethylsilane. The ranges of the concentration ratios of the top five species to  
377 all the upper-altitude VOCs at sites 1, 2, and 3 were 56.0%–68.5% (average = 61.5%), 51.7%–72.6%  
378 (average = 60.1%), and 54.1%–67.9% (average = 59.5%), respectively. The predominance of the top  
379 five species in the total upper-altitude VOC concentration in field measurement 2 was lower than that  
380 in field measurement 1, which was because more VOCs were detected in field measurement 2 than  
381 in field measurement 1.

382 2,4-Dimethyl heptane and toluene had the highest and second-highest concentrations among the  
383 VOCs at sites 1 and 3, respectively. However, at site 2, they had the second- and third-highest  
384 concentrations, respectively, with propyl propionate having the highest concentration. Toluene is the  
385 most common organic compound and originates from vehicle exhaust and industrial emissions. At  
386 each site, the detected concentrations of industrial organic solvents, such as benzene, xylene,  
387 ethylbenzene, butanone, acetone, isopropyl alcohol, and ethyl acetate, were higher in field  
388 measurement 2 than in field measurement 1. Isopropyl alcohol is a crucial cleaning agent and  
389 disinfectant in high-tech factories. The second largest high-tech park in Taiwan is located  
390 approximately 4 km north of the study area. Thus, a considerable quantity of the toluene detected in  
391 field measurement 2 originated from industrial emissions. 2,4-Dimethylheptane is a crucial  
392 component of high-octane fuel, such as gasoline; thus, the detected 2,4-dimethylheptane content  
393 mainly originated from vehicle emissions. Hexamethylcyclotrisiloxane is used as an additive in the  
394 creation of plastic and rubber products, paints, adhesives, cosmetics, food packaging, and many other  
395 products; thus, the detected hexamethylcyclotrisiloxane content probably originated from TIP and  
396 TPMP (Fig. 4). Tetramethylsilane is used as a starting material for synthesizing more complex  
397 organosilanes, and the tetramethylsilane detected in field measurement 2 might have also originated  
398 from TIP and TPMP. In addition, propyl propionate is a safer substitute for toluene because of its low  
399 odor, moderately volatile nature, and nonhazardous and nonpolluting ester product; thus, the propyl  
400 propionate detected in field measurement 2 mainly originated from industrial emissions. Alkanes  
401 were the dominant VOCs at various altitudes and sites in field measurement 2. Thus, concentrations  
402 of the VOCs originating from vehicle exhaust might have been higher than those of the VOCs  
403 originating from industrial exhaust, which is in line with the results of field measurement 1. The order  
404 of average VOC concentrations at the three sites in field measurement 2 was as follows: site 3 > site  
405 1 > site 2. This order differed from that in field measurement 1, and this difference was probably  
406 because the prevailing winds in the study area changed from north–northeast in field measurement 1  
407 to northeast by east in field measurement 2.

#### 408 **4 Discussion**

409 In this study, a UAV platform with sensing and sampling systems was developed for 3D air  
410 pollutant concentration measurements. This platform was used in two measurement periods for

411 detecting air pollutant concentrations in a large special industrial zone that includes a traditional  
412 industrial park, a precision machinery park, and a municipal waste incineration plant. To elucidate  
413 the transport of air pollutants in the aforementioned industrial zone, this study used a single theodolite  
414 on the ground to measure the speeds and directions of the upper winds during the field measurement  
415 periods. The use of this method prevented the airflow caused by the rotor of the UAV from influencing  
416 the measurements. The measurement results obtained by the sensing system of the developed  
417 platform, which contains multiple microsensors and is integrated with IoT technology, demonstrated  
418 the feasibility of this platform for determining the real-time 3D distributions of critical air pollutants.  
419 The NO<sub>2</sub> and O<sub>3</sub> contents were 0 ppm in the two field measurements because the sensitivities of the  
420 NO<sub>2</sub> and O<sub>3</sub> sensors were too low. All VOC concentrations at the three field measurement sites were  
421 very low ( $\leq 0.02$  ppm), possibly because the sensitivity of the VOC sensor was also too low. The sum  
422 of the O<sub>3</sub> and NO<sub>2</sub> concentrations ( $[O_3] + [NO_2]$ ) is defined as odd oxygen (ODO) in atmospheric  
423 chemistry (Yee et al., 2021; Zhang et al., 2018). Many studies have indicated that a high positive  
424 correlation exists between the concentrations of ODO and secondary organic aerosols (SOA's)  
425 (Hernod et al., 2008; Wood et al., 2010; Hu et al., 2016); thus, the concentration of SOA can be  
426 represented by the sum of the O<sub>3</sub> and NO<sub>2</sub> concentrations. SOA can have detrimental effects on the  
427 health and mortality of patients with chronic inflammatory diseases (Déméautis et al., 2022).  
428 Therefore, developing highly sensitive O<sub>3</sub>, NO<sub>2</sub>, and VOC microsensors is desirable for improving  
429 UAV air pollutant telemetry.

430 The sampling system of the developed platform, which contains multiple remote-controllable  
431 gas sampling sets, can conduct multipoint sampling according to the relevant situation for analyzing  
432 the composition of air pollutants. The results show that it is feasible to replace a canister with the  
433 sampling bag 1-L Tedlar bag for the 3D measurement of VOC concentrations according to the  
434 procedures of the TO-15 method of the US EPA. Moreover, the three air pumps of the gas sampling  
435 kits are connected in parallel to a length of 60-cm vertical sampling tube at the top of the UAV. The  
436 sampling tube was at the top of the UAV because the propeller causes downwash when UAV is close  
437 to the ground (Yang et al., 2020). In addition, the dispersion effects of drone propellers are small in  
438 the monitoring of atmospheric pollutants (Fan et al., 2023) but cause a large negative bias in the  
439 measurement of pollutant concentrations in plumes. (Villa et al., 2016). Therefore, the arrangement  
440 of the vertical sampling pipe is acceptable.

441 The observation and analysis data obtained from the single-theodolite method, sensing system,  
442 and sampling system were used to examine the effect of air pollutant discharge from the investigated  
443 industrial zone on the study area. The results of this study indicate the feasibility of using the  
444 developed UAV platform to accurately identify pollutants and determine their 3D spatial distributions  
445 concentrations in a study area. Thus, the UAV platform can serve as a useful tool in the management  
446 and decision-making process of air pollution in industrial areas.

## 447 5 Conclusions

448 Most research on the application of UAV systems in air pollution monitoring has focused on the  
449 development of microsensors and control and communication systems; few studies have used UAV

450 systems for the sampling and analysis of **low-altitude pollutants near the ground level**. Therefore, in  
451 the present study, a UAV platform with sensing and sampling systems was developed for 3D air  
452 pollutant concentration measurements. The sensing system of this platform contains multiple  
453 microsensors and IoT technologies for obtaining the real-time 3D distributions of critical air  
454 pollutants. The sampling system contains multiple remote-controllable gas sampling sets as sampling  
455 devices, and these sampling sets contain a 1-L Tedlar bag instead of a canister for the 3D measurement  
456 of VOC concentrations in accordance with the TO-15 method of the US EPA. The developed platform  
457 was used to detecting air pollutant emissions in a large special industrial zone that includes a  
458 traditional industrial park, precision machinery park, and municipal waste incineration plant.  
459 According to the local prevailing wind direction in the study area, three field measurement sites were  
460 selected—one site located upwind and two sites located downwind. Comprehensive air pollutant  
461 characterization was performed in the aforementioned industrial zone during two field measurements  
462 in March and May 2023. The results of this characterization indicate that the developed UAV platform  
463 can accurately obtain the 3D concentration distributions of critical air pollutants in real time and  
464 conduct multipoint sampling according to the relevant situation for analyzing the composition of air  
465 pollutants.

466 *Data availability.* Data not available - participant consent.

467 *Author contributions.* JWL developed the concept and methodology for this work. JWL and CHS  
468 processed the field measurements data collected, and analysis of the samples. JWL provided scientific  
469 expertise on in situ data. Data handling and analysis were performed by CHS with contributions from  
470 JWL. All authors contributed to the proofreading and added valuable suggestions to the final draft.

471 *Competing interests.* The contact author has declared that none of the authors has any competing  
472 interests.

473 *Acknowledgments.* The authors gratefully acknowledgments distinguished Professor Jeng-Jong  
474 Liang, Feng Chia University, Taiwan, for providing the air pollution expertise and using his gas  
475 chromatography/mass spectrometry; and like to thank Green Ideas Synergy Co., Taiwan, for  
476 providing the micro sensors and using company's IoT framework for this research.

477 *Financial support.* This research has been supported by the Taichung City Environmental Protection  
478 Bureau, Taiwan, for financially supporting this research under Taichung EPB-P1111017073.

## 479 **References**

- 480 Alvarado, M., Gonzalez, F., Fletcher, A., Doshi, A.: Towards the development of a low cost airborne  
481 sensing system to monitor dust particles after blasting at open-pit mine sites. *Sensors* 15,  
482 19667–19687, <https://doi.org/10.3390/s150819667>, 2015.
- 483 Arroyo, P., Gómez-Suárez, J., Herrero, J. L., Lozano, J.: Electrochemical gas sensing module  
484 combined with Unmanned Aerial Vehicles for air quality monitoring. *Sens. Actuators B. Chem.*  
485 364, 131815, <https://doi.org/10.1016/j.snb.2022.131815>, 2022.

- 486 Boursianis, A. D., Papadopoulou, M. S., P. Diamantoulakis, et al.: Internet of Things (IoT) and  
487 Agricultural Unmanned Aerial Vehicles (UAVs) in smart farming: A comprehensive review.  
488 Internet of Things 18, 100187, <https://doi.org/10.1016/j.iot.2020.100187>, 2022.
- 489 Cozma, A., Firculescu, A. C., Tudose, D., Ruse, L.: Autonomous multi-rotor aerial platform for air  
490 pollution monitoring. *Sensors* 22(3), 860, <https://doi.org/10.3390/s22030860>, 2022.
- 491 De Fazio, R., Matteo Dinoi, L., De Vittorio, M., Visconti, P.: A sensor-based drone for pollutants  
492 detection in Eco-Friendly Cities: Hardware design and data analysis application. *Electronics* 11,  
493 52, <https://doi.org/10.3390/electronics11010052>, 2022.
- 494 Déméautis, T., Delles, M., Tomaz, S., Monneret, G., Glehen, O., Devouassoux, G., George, C.,  
495 Bentaher, A.: Pathogenic mechanisms of secondary organic aerosols. *Chem. Res. Toxicol.* 35(7),  
496 1146–1161, <https://doi.org/10.1021/acs.chemrestox.1c00353>, 2022.
- 497 Duangsuwan, S., Prapruetdee, P., Subongkod, M., Klubsuwan, K.: 3D AQI mapping data assessment  
498 of low-altitude drone real-time air pollution monitoring. *Drones* 6, 191,  
499 <https://doi.org/10.3390/drones6080191>, 2022.
- 500 Fan, G., Liu, Z., Qin, Y., Long, B., Li, H., Li, J.: Airflow characteristics of rotorcraft plant protection  
501 UAV operating in rice fields. *Biosyst. Eng.* 226, 209–222,  
502 <https://doi.org/10.1016/j.biosystemseng.2023.01.007>, 2023.
- 503 Fumian, F., Chierici, A., Bianchelli, M., Martellucci, L., Rossi, R., Malizia, A., Gaudio, P., d'Errico,  
504 F., Giovanni D.D.: Development and performance testing of a miniaturized multi-sensor system  
505 combining MOX and PID for potential UAV application in TIC, VOC and CWA dispersion  
506 scenarios. *Eur. Phys. J. Plus* 136, 913, <https://doi.org/10.1140/epjp/s13360-021-01858-2>, 2021.
- 507 Fumian, F., Giovanni, D.D., Martellucci, L., Rossi, R., Gaudio, P.: Application of miniaturized  
508 sensors to unmanned aerial systems, a new pathway for the survey of polluted areas: preliminary  
509 results. *Atmosphere* 11, 471, <https://doi.org/10.3390/atmos11050471>, 2020.
- 510 Galle, B., Arellano, S., Bobrowski, N., et. al.: A multi-purpose, multi-rotor drone system for long-  
511 range and high-altitude volcanic gas plume measurements. *Atmos. Meas. Tech.* 14, 4255–4277,  
512 <https://doi.org/10.5194/amt-14-4255-2021>, 2021.
- 513 Gu, Q., Jia, C.: A consumer UAV-based air quality monitoring system for smart cities. 2019 IEEE  
514 International Conference on Consumer Electronics (ICCE), DOI: 10.1109/ICCE.2019.8662050,  
515 2019.
- 516 Gu, Q., Michanowicz, D. R., Jia, C.: Developing a modular unmanned aerial vehicle (UAV) platform  
517 for air pollution profiling. *Sensors* 18, 4363, <https://doi.org/10.3390/s18124363>, 2018.
- 518 Herndon, S. C., Onasch, T. B., Wood, E. C., Kroll, J. H., et al.: Correlation of secondary organic  
519 aerosol with odd oxygen in Mexico City. *Geophys. Res. Lett.* 35, 15804,  
520 [doi:10.1029/2008GL034058](https://doi.org/10.1029/2008GL034058), 2008.
- 521 Hu, W., Hu, M., Hu, W., Jimenez, J. L., Yuan, B., Chen, W., et al.: Chemical composition, sources,  
522 and aging process of submicron aerosols in Beijing: Contrast between summer and winter. *J.*  
523 *Geophys. Res. Atmos.* 121 (2016) 1955–1977, <https://doi.org/10.1002/2015JD024020>, 2016.
- 524 Huang, F., Peng, S., Yang, H., Cao, H., Ma, N., Ma, L.: Development of a novel and fast XRF



525 instrument for large area heavy metal detection integrated with UAV. *Environ. Res.* 214, 113841,  
526 <https://doi.org/10.1016/j.envres.2022.113841>, 2022.

527 Leitner, S., Feichtinger, W., Mayer, S., Mayer, F., Krompetz, D., Hood-Nowotny, R., Watzinger, A.:  
528 UAV-based sampling systems to analyse greenhouse gases and volatile organic compounds  
529 encompassing compound-specific stable isotope analysis. *Atmos. Meas. Tech.*, 16, 513–527  
530 <https://doi.org/10.5194/amt-16-513-2023>, 2023.

531 Liu, C., Huang, J., Wang, Y., Tao, X., Hu, C., Deng, L., Xu, J., Xiao, H. W., Luo, L., Xiao, H. Y., Xiao,  
532 W.: Vertical distribution of PM<sub>2.5</sub> and interactions with the atmospheric boundary layer during the  
533 development stage of a heavy haze pollution event. *Sci. Total Environ.* 704, 135329,  
534 <https://doi.org/10.1016/j.scitotenv.2019.135329>, 2020.

535 Middleton, W. E. K., Spilhaus A. F.: *Meteorological Instruments*. 3<sup>rd</sup> ed., Heritage: University of  
536 Toronto Press. pp181-183. [doi.org/10.3138/9781487572013-056](https://doi.org/10.3138/9781487572013-056), 2019.

537 Noori, R., Dahnil, D. P.: The effects of speed and altitude on wireless air pollution measurements  
538 using hexacopter drone. (IJACSA) *Int. J. Adv. Comput. Sci. Appl.* 11(9), 268-276,  
539 (DOI): 10.14569/IJACSA.2020.0110931, 2020.

540 Pochwała, S., Gardecki, A., Lewandowski, P., Somogyi, V., Anweiler, S.: Developing of low-cost air  
541 pollution sensor—Measurements with the unmanned aerial vehicles in Poland. *Sensors* 20, 3582,  
542 <https://doi.org/10.3390/s20123582>, 2020.

543 Pounds, P.E.I., Bersak, D.R., Dollar, A.M.: *Grasping from the air: Hovering capture and load stability.*  
544 *2011 IEEE ICRA SHICC, May, 2011, Shanghai, China. DOI: 10.1109/ICRA.2011.5980314, 2011.*

545 Qiu, S., Chen, B., Wang, R., Zhu, Z., Wang, Y., Qiu, X.: Estimating contaminant source in chemical  
546 industry park using UAV-based monitoring platform, artificial neural network and atmospheric  
547 dispersion simulation. *RSC Adv.* 7, 39726–39738, <https://doi.org/10.1039/C7RA05637K>, 2017.

548 Samad, A., Florez, D.A., Chourdakis, I., Vogt, U.: Concept of using an unmanned aerial vehicle (UAV)  
549 for 3D investigation of air quality in the atmosphere—Example of measurements near a roadside.  
550 *Atmosphere* 13, 663, <https://doi.org/10.3390/atmos13050663>, 2022.

551 Shen, L., Cheng, Y., Bai, X., Dai, H., et al.: Vertical profile of aerosol number size distribution during  
552 a haze pollution episode in Hefei, China. *Sci. Total Environ.* 814, 152693,  
553 <https://doi.org/10.1016/j.scitotenv.2021.152693>, 2022.

554 Singh, P. K., Sharma, A.: An intelligent WSN-UAV-based IoT framework for precision agriculture  
555 application. *Comput. Electr. Eng.* 100, 107912,  
556 <https://doi.org/10.1016/j.compeleceng.2022.107912>. 2022.

557 Sun, X., Zhao, T., Tang, G., Bai, Y., et al.: Vertical changes of PM<sub>2.5</sub> driven by meteorology in the  
558 atmospheric boundary layer during a heavy air pollution event in central China. *Sci. Total Environ.*  
559 858, 159830, <https://doi.org/10.1016/j.scitotenv.2022.159830>, 2023.

560 Suroto, A., Ubaidillah, A., Ulum, M.: Air condition monitoring using way point based UAV  
561 (Unmanned Aerial Vehicle). *Int. J. Sci. Eng. Inf. Technol.* 3(1), 109–114,  
562 <https://journal.trunojoyo.ac.id/ijseit>, 2018.

563 Yang, S., Tang, Q., Zheng, Y., Liu, X., Chen, J.,ation of a six-rotor UAV downwash,» *Int. J. Agric.*

564 Biol. Eng.13(4),10–18, 2020

565 Villa, T. F., Salimi, F., Morton, K., Morawska, L., Gonzalez, F.: Development and validation of a  
566 UAV based system for air pollution measurements. *Sensors* 16, 2202,  
567 <https://doi.org/10.3390/s16122202>, 2016.

568 Wood, E. C., Canagaratna, M. R., Herndon, S. C., et al.: Investigation of the correlation between odd  
569 oxygen and secondary organic aerosol in Mexico City and Houston. *Atmos. Chem. Phys. Discuss.*  
570 10 (2010) 8947–8968, <https://doi.org/10.5194/acp-10-8947-2010>, 2010.

571 Xie, T., Liu, R., Hai, R. T., Hu, Q. H., Lu. Q.: UAV platform based atmospheric environmental  
572 emergency monitoring system design. *J. Appl. Sci.* 13(8), 1289–1296,  
573 <https://doi:10.3923/jas.2013.1289.1296>, 2013.

574 Yang, S., Tang, Q., Zheng, Y., Liu, X., Chen, J., Li, X.: Model migration for CFD and verification of  
575 a six-rotor UAV downwash. *Int. J. Agric. Biol. Eng.*13(4) 10–18, DOI:  
576 [10.25165/j.ijabe.20201304.5569](https://doi.org/10.25165/j.ijabe.20201304.5569), 2020.

577 Yang, Z., Yu, X., Dedman, S., Rosso, M., Zhu, J., Yang, J., Xia, Y., Tian, Y., Zhang, G., Wang, J.:  
578 UAV remote sensing applications in marine monitoring: Knowledge visualization and review. *Sci.*  
579 *Total Environ.* 838, 155939, <https://doi.org/10.1016/j.scitotenv.2022.155939>, 2022.

580 Yee, L. D., Craven, J. S., Loza, C. L., Schilling, K. A., Ng, N. L., et al.: Secondary organic aerosol  
581 formation from low-NO<sub>x</sub> photooxidation of dodecane: evolution of multigeneration gas-phase  
582 chemistry and aerosol composition, *J. Phys. Chem. A* 116(24), 6211–6230,  
583 <https://doi.org/10.1021/jp211531h>, 2011.

584 Yee, L., Pollak, W., Brunt, D., et al.: A new theodolite for following fast moving objects especially  
585 for making pilot balloon observations of greater accuracy. *Q. J. R. Meteorol. Soc.* 65, 443–447,  
586 <https://doi.org/10.1002/qj.49706528117>, 1939.

587 Yungaicela-Naula, N. M., Garza-Castañón, L. E., Mendoza-Domínguez, A., Minchala-Avila, L. I.,  
588 Garza-Elizondo, L. E.: Design and implementation of an UAV-based platform for air pollution  
589 monitoring and source identification. 2017 Congreso Nacional de Control Automático, Monterrey,  
590 Nuevo León, Mexico. <https://amca.mx/memorias/amca2017/media/files/0041.pdf>, 2017.

591 Zhang, C., Lu, X. H., Zhai, J. H., Chen, H., Yang, X., Zhang, Q., et al.: Insights into the formation of  
592 secondary organic carbon in the summertime in urban Shanghai. *J Environ Sci -China.* 72, 118–  
593 132, <https://doi.org/10.1016/j.jes.2017.12.018>, 2018.

594 Zheng, T., Li, B., Li, X. B., Wang, Z., Li, S. Y., Peng, Z. R.: Vertical and horizontal distributions of  
595 traffic-related pollutants beside an urban arterial road based on unmanned aerial vehicle  
596 observations. *Build. Environ.* 187, 107401, <https://doi.org/10.1016/j.buildenv.2020.107401>, 2021.

597 Zhu, X., Zhu, X., Rui Yan, R., Peng R.: Optimal routing, aborting and hitting strategies of UAVs  
598 executing hitting the targets considering the defense range of targets. *Reliab. Eng. Syst. Saf.* 215,  
599 [107811, https://doi.org/10.1016/j.ress.2021.107811](https://doi.org/10.1016/j.ress.2021.107811), 2021.